

Screen-based analysis of magnetic nanoparticle libraries formed using peptidic iron oxide ligands

Mariya Barch, Satoshi Okada, Benjamin B. Bartelle, & Alan Jasanoff

SUPPLEMENTAL INFORMATION

| Table of Contents | Page |
|--|-------------|
| Table S1. Relative absorbance of peptide-IONP suspensions following ligand exchange in water | S2 |
| Figure S1. Stability of selected peptide-IONP complexes at low ionic strength | S3 |
| Figure S2. Transmission electron microscopy of CDDZ-IONP in negative stain | S4 |
| Figure S3. Determination of the zeta potential of a peptide-IONP complex | S5 |
| □ Figure S4. Characterization of library peptide-IONP complexes by MRI and DLS | S6 |
| Figure S5. Analysis of r_2 consistency over time | S7 |
| Supplemental Methods | S8 |

Table S1. Relative absorbance of peptide-IONP suspensions following ligand exchange in water*

| <i>ligand</i> | <i>rel. absorbance</i> | <i>ligand</i> | <i>rel. absorbance</i> |
|------------------|------------------------|---------------|------------------------|
| no peptide | 0.18 ± 0.02 | SSSDSSSDZ | 0.41 ± 0.06 |
| citrate | 0.38 ± 0.06 | SSSDZ | 0.41 ± 0.04 |
| CDDZ | 0.47 ± 0.02 | SSSDZDSSS | 0.45 ± 0.07 |
| DDDDKDDZ | 0.37 ± 0.08 | SSSKSSDDZ | 0.58 ± 0.12 |
| DDSSSSSSZ | 0.29 ± 0.09 | SSSSDDZ | 0.44 ± 0.06 |
| DSPHRHS | 0.15 ± 0.02 | SSSSDDZDZDZ | 0.65 ± 0.08 |
| DSPHRHSZ | 0.08 ± 0.02 | SSSSDDZZ | 0.57 ± 0.11 |
| DSSSSSSDZ | 0.39 ± 0.04 | SSSSDDZZZ | 0.68 ± 0.17 |
| DYKDDDDKSSDDZ | 0.40 ± 0.05 | SSSSDDZZZZ | 0.66 ± 0.14 |
| EEEEEE | 0.12 ± 0.00 | SSSSDPGGDDZ | 0.42 ± 0.04 |
| GRKKRRQRRRPQCDDZ | 0.03 ± 0.01 | SSSSLLLLZ | 0.06 ± 0.02 |
| GSGSGSDDZ | 0.44 ± 0.04 | SSSSLLSSZ | 0.19 ± 0.16 |
| HHHHHHCDDZ | 0.12 ± 0.02 | SSSSSDGDCZ | 0.40 ± 0.02 |
| HHHHHHDDZ | 0.42 ± 0.06 | SSSSSGCDDZ | 0.38 ± 0.04 |
| SEEE | 0.11 ± 0.01 | SSSSSKDDZ | 0.43 ± 0.02 |
| LRRASLGDDZ | 0.04 ± 0.00 | SSSSSSDDZ | 0.45 ± 0.01 |
| LSTVQTISPSNH | 0.07 ± 0.02 | SSSSSSDDZ | 0.38 ± 0.08 |
| LSTVQTISPSNHZ | 0.07 ± 0.01 | SSSSSSDDY | 0.10 ± 0.02 |
| NHWSDKRAQITI | 0.19 ± 0.13 | SSSSSSEEZ | 0.43 ± 0.06 |
| PGAAHYGSSDDZ | 0.41 ± 0.08 | SSSSSSLLZ | 0.05 ± 0.01 |
| RADARADAZ | 0.07 ± 0.00 | SSSSSSRRZ | 0.08 ± 0.05 |
| RADAZ | 0.13 ± 0.02 | SSSSSSSDZ | 0.33 ± 0.12 |
| RRRADDSDDDDDZ | 0.45 ± 0.07 | SSSSSSSSSSSZ | 0.11 ± 0.01 |
| SGSSGSDDDZ | 0.42 ± 0.06 | SSSSSSSSSZ | 0.13 ± 0.02 |
| SGSSSSDDZ | 0.39 ± 0.06 | SSSSSZ | 0.12 ± 0.01 |
| SSDDZ | 0.41 ± 0.05 | WSHPQFEKDDZ | 0.17 ± 0.06 |
| SSSCDDZ | 0.80 ± 0.15 | ZDDSSDDZ | 0.07 ± 0.02 |
| SSSCEEZ | 0.71 ± 0.14 | ZDDSSSSSS | 0.33 ± 0.06 |
| SSSDSSSZ | 0.37 ± 0.05 | ZDDSSSSSSSDZ | 0.40 ± 0.17 |
| SSSDSSSDZ | 0.41 ± 0.06 | | |

*Candidate ligands (50 μ M) were complexed with IONP cores (4.2 mM Fe) as described in the Methods section. Relative absorbance measurements indicate peptide ligands' ability to prevent pelleting of IONP complexes following 30 s centrifugation at 2,000 g, and thus reflect colloidal stability. No ligand and citrate conditions represent negative and positive control conditions, respectively. Error margins reflect s.e.m. of three independent measurements.

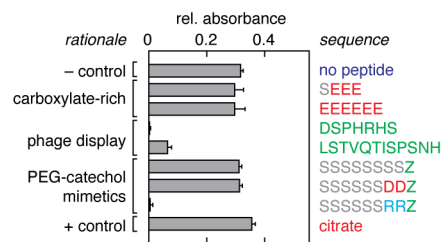


Figure S1. Stability of selected peptide-IONP complexes at low ionic strength. Relative absorbance values measured in 12 mM phosphate buffer, pH 7.4, without added salt, are presented in analogy to Fig. 1b.

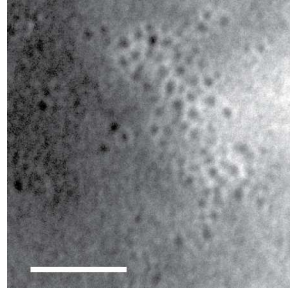


Figure S2. Transmission electron microscopy of CDDZ-IONP in negative stain. A representative field of view visualized with contrast arising from iron oxide cores and phosphotungstic acid. Scale bar = 50 nm.

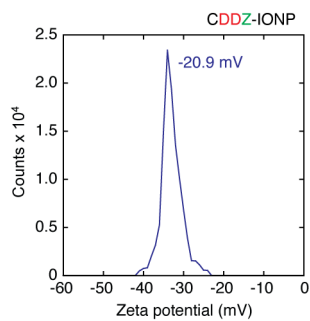


Figure S3. Determination of the zeta potential of a peptide-IONP complex. An aqueous suspension of CDDZ-IONP (300 μM Fe, 3 μM peptide) was analyzed by laser Doppler micro-electrophoresis. A histogram of the computed zeta potential distribution is shown, with its peak at -20.9 mV.

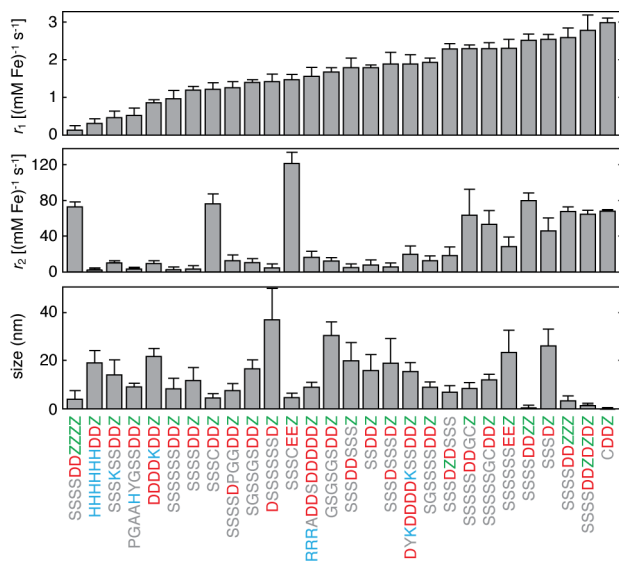


Figure S4. Characterization of library peptide-IONP complexes by MRI and DLS. All complexes included 500 μM Fe and 5 μM peptide, and displayed retention in suspension after centrifugation, as judged by OD₄₅₀ analysis, indicating relative stability in PBS. Top, middle, and bottom panels report r_1 , r_2 , and radius values, respectively, for peptide sequences noted at bottom. Radius values determined by cumulant fitting to raw DLS data were scaled according to the mass-weighted radius measured from CDDZ-IONP (5 nm). Error bars denote s.e.m. of three independent measurements.

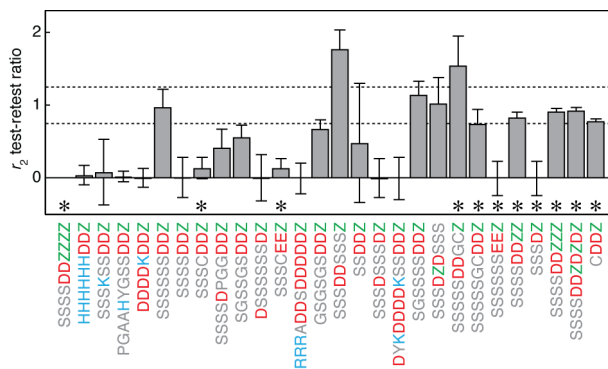


Figure S5. Analysis of r_2 consistency over time. The ratio of r_2 values measured before and after a 30 minute room temperature incubation period are reported. Peptides included in this analysis were those that produced stable colloids as judged by resistance to pelleting by centrifugation after preparation, as in Fig. 2 and Fig. S2. Peptides that produced r_2 values greater than $30 \text{ (mM Fe)}^{-1} \text{ s}^{-1}$ are marked with asterisks. Four peptides produced IONP complexes with both high r_2 values and test-retest ratios within plus or minus 20% of one (values contained between dotted lines shown); properties of these optimized complexes are reported in Fig. 2b.

SUPPLEMENTAL METHODS

Materials and reagents. C-terminally amidated peptides used in this work were synthesized according to standard F-moc chemistry by the MIT biopolymers facility. Analytical HPLC and MALDI were used to assess peptide purity. Peptide solutions were prepared by dilution to appropriate concentration in water. All other chemicals were purchased from Sigma-Aldrich (St. Louis, MO). Mineral cores used in iron oxide nanoparticle (IONP) formulation had a reported diameter of 5 nm and were obtained from Sigma-Aldrich as oleate complexes in toluene, at a concentration of 5 mg/mL IONP.

Preparation of peptide-IONP complexes. IONP cores were extracted from toluene into tetramethylammonium (TMA) by mixing 2 mL of the stock suspension in toluene with 2 mL of 1.7% TMA in water¹. TMA facilitates the interaction of aqueous and organic phases and promotes emulsification. Aqueous and organic phases were allowed to separate naturally over the course of several hours. Once separation was complete, the aqueous layer was dark brown and the organic toluene layer was clear. The aqueous layer was isolated, and IONPs were precipitated with acetone several times to wash away residual oleic acid and ultimately resuspended in 0.1% TMA. TMA-stabilized aqueous IONP suspensions containing 45 mM Fe were obtained using this procedure and were stored at room temperature for up to 6 months. To form peptide-IONP complexes, IONP stock solutions were diluted to 14 mM Fe and mixed in 3:1 volume ratio with stock peptide solutions at 500 μ M. Resulting mixtures were then diluted with water and 10x phosphate buffered saline (PBS) to a final iron concentration of 4.2 mM in 1x PBS, pH 7.4. Positive and negative control preparations were produced by substituting 500 μ M citrate or water, respectively, for peptide solutions. Iron concentrations in IONP preparations were measured using OD₄₅₀, interpreted based on an extinction coefficient of 430 cm⁻¹ (M Fe)⁻¹, which was determined by comparison of absorbance measurements to calibrated elemental analysis performed by inductively coupled plasma optical emission spectroscopy.

Sample characterization. Colloidal stability of peptide-IONP complexes was evaluated following formulation by examining OD₄₅₀ after centrifugation at 2,000g for 30 s. Samples that showed OD₄₅₀ values within 30% of maximum were judged as stable and used for subsequent experiments. For display purposes, relative absorbance values were computed from each set of peptides by scaling absolute OD₄₅₀ measurements to the average of values for three defined reference complexes. Dynamic light scattering (DLS) was used to evaluate IONP sizes. Measurements were performed at room temperature on a DynaPro DLS system (Wyatt Technology, Santa Barbara, CA). Reported measurements of absolute radius were obtained using mass-weighted analysis of scattering correlograms using the Dynamics 6.7.7.9 software package (Wyatt). Relative radius measurements for peptide-IONP libraries were obtained using cumulant analysis, which is independent of model parameters; for display in Figs. 2 and S4, values were scaled to the mass-weighted DLS radius of CDDZ-IONP (5 nm).

Stability of CDDZ-IONP in biological buffer was measured by acquiring absorbance spectra over a wavelength range from 350-750 nm in a Nanodrop ND-1000 spectrometer (Wilmington, DE) at multiple time points during incubation at room temperature in 10% fetal bovine serum (Life Technologies, Grand Islands, NY) formulated in PBS.

Transmission electron microscopy (TEM) was performed using a JEOL JEM-2010 high-resolution transmission electron microscope (JEOL USA, Peabody, MA). Samples were prepared as described above and yielding a final OD₄₅₀, of 0.05; 5 μ L of this suspension was applied to a 200 μ m mesh TEM grid (Electron Microscopy Sciences, Hatfield, PA) and desiccated for analysis. Samples in negative stain were prepared by adding three 5 μ L aliquots of nanoparticle solution successively on a TEM grid, each followed by blotting to remove excess liquid and 20 min. drying at room temperature. Then three 10 μ L aliquots of a negative staining solution (2% phototungstic acid, pH 7) were applied in succession, each again followed by blotting and 20 min. drying. The sample was then further dried overnight and imaged on a JEOL JEM-200CX microscope.

Zeta potential measurement was performed by laser Doppler micro-electrophoresis using a Malvern Zetasizer Nano ZS90 equipped with a dip cell kit (Malvern, United Kingdom). Samples consisted of CDDZ-IOPN formulated in deionized water with a total iron concentration of 300 μ M. Data were displayed and analyzed using the manufacturer's software.

Magnetic resonance imaging (MRI) was performed on a Bruker Avance III 7 T scanner (Bruker Instruments, Ettlingen, Germany), using a 12 cm outer diameter Bruker birdcage transceiver. Relaxivity measurements and images were obtained from samples arrayed into split 384-well microtiter plates, with IONP concentrations of 0.1-0.5 mM Fe. Data from 2 mm vertically-centered horizontal slices with 5.5 x 5.5 or 6.0 x 6.0 cm fields of view and 256 x 256 matrix sizes were obtained using T_1 - and T_2 -weighted multislice multiecho spin echo (MSME) pulse sequences with repetition time (TR) = 73-3125 ms and echo time (TE) = 10-300 (30 echoes, 10 ms echo spacing). Data were reconstructed and analyzed using custom routines in Matlab (Mathworks, Natick, MA). Relaxivity values were obtained by computing T_1 and T_2 relaxation rates from image data and determining the slope of the relationship between relaxation rate and iron concentration across sample dilutions.

***In vivo* imaging.** Swiss Webster mice were anesthetized with 1.5% isoflurane and imaged using a Bruker 7 T scanner with a birdcage transceiver. Scans were performed before, 1 h after, and 12 h after tail vein injection of 150 μ L of CDDZ-IONP with iron concentration of 4 mM in PBS. T_2 -weighted imaging and relaxation rate measurements were performed using an MSME pulse sequence with TR = 2500 ms and TE = 11-176 ms (16 echoes, 11 ms echo spacing). Data were acquired over coronal slices with 2 mm slice thickness and 200 μ m in-plane resolution. Image reconstruction, analysis, and display were performed using Matlab and ImageJ (National Institutes of Health, Bethesda, MD). Region of interest (ROI) analysis of T_2 values was performed by averaging data from elliptical ROIs of approximately 1 mm x 0.75 mm manually placed over perispinal muscle in each individual image.

Data analysis and display. Additional data analysis was performed using the R statistical package (University of Auckland, New Zealand) and Igor Pro 6.03A2 (Wavemetrics, Lake Oswego, OR). Figures were generated using Adobe Illustrator (Adobe Systems, San Jose, CA). All error bars represent standard errors of the mean over multiple independent measurements, unless otherwise stated.